DMD Fast Forward. Published on July 27, 2005 as doi:10.1124/dmd.105.004903

IN VITRO METABOLISM OF THE CALMODULIN ANTAGONIST DY-9760e BY HUMAN LIVER MICROSOMES: INVOLVEMENT OF CYTOCHROME P450s IN ATYPICAL KINETICS AND POTENTIAL DRUG INTERACTIONS

SHUKO TACHIBANA, YUKO FUJIMAKI, HIROYUKI YOKOYAMA, OSAMU OKAZAKI, and KEN-ICHI SUDO

Drug Metabolism and Physicochemistry Research Laboratories, R&D Division, Daiichi Pharmaceutical Co., Ltd., Tokyo, Japan (S.T., Y.F., O.O., K.S); Mitsubishi Chemical Safety Institute Ltd., Kashima Laboratory, Ibaraki, Japan (H.Y.)

Running title: **Atypical Metabolic Kinetics of DY-9760e**

The corresponding author: Shuko Tachibana; Drug Metabolism & Physicochemistry Research Laboratories, R&D Division, Daiichi Pharmaceutical Co., Ltd., 1-16-13, Kita-kasai, Edogawa-ku, Tokyo 134-8630, Japan. Telephone: (3) 3680-0151; fax: (3) 5696-8228; e-mail: tachiroq@daiichipharm.co.jp

The number of text pages :	33
Number of tables :	3
Number of figures :	5
Numbers of references :	39
Number of words in the Abstract :	217
Number of words in the Introduction :	387
Number of words in the Discussion :	1381

Abbreviations: CYP, cytochrome P450; DY-9760e, 3-[2-[4-(3-chloro-2-methylphenyl)-1-piperazinyl]ethyl]-5,6-dimethoxy-1-(4-imidazolyl methyl)-1*H*-indazole dihydrochloride 3.5 hydrate; DY-9836, 3-[2-[4-(3-chloro-2-methylphenyl)-1-piperazinyl]ethyl]-5,6-dimethoxy-1*H*-indazole; LC-MS, liquid chromatography-mass spectrometry; APCI, atmospheric pressure chemical ionization; SIM, selected ion monitoring; b_5, cytochrome b_5; L-B plot, Lineweaver-Burk plot.

DMD Fast Forward. Published on July 27, 2005 as DOI: 10.1124/dmd.105.004903
This article has not been copyedited and formatted. The final version may differ from this version.

ABSTRACT

Human cytochrome P450 (CYP) isozyme(s) responsible for metabolism of the calmodulin antagonist DY-9760e and kinetic profiles for formation of its 6 primary metabolites (M3, M5, M6, M7, M8, and DY-9836) were identified using human liver microsomes and recombinant CYP enzymes. In vitro experiments, including an immunoinhibition study, correlation analysis, and reactions with recombinant CYP enzymes, revealed that CYP3A4 is the primary CYP isozyme responsible for the formation of the DY-9760e metabolites, except for M5, which is metabolized by CYP2C9. Additionally, at clinically relevant concentrations, CYP2C8 and 2C19 make some contribution to the formation of M3 and M5, respectively. The formation rates of DY-9760e metabolites except for M8 by human liver microsomes are not consistent with a Michaelis-Menten kinetics model, but are better described by a substrate inhibition model. In contrast, the enzyme kinetics for all metabolites formed by recombinant CYP3A4 can be described by an autoactivation model or a mixed model of autoactivation and biphasic kinetics. Inhibition of human CYP enzymes by DY-9760e in human liver microsomes was also investigated. DY-9760e is a very potent competitive inhibitor of CYP2C8, 2C9 and 2D6 (K_i 0.25–1.7 μM); a mixed competitive and non-competitive inhibitor of CYP2C19 (K_i 2.4 μM); and a moderate inhibitor of CYP1A2 and 3A4 (K_i 11.4–20.1 μM), suggesting a high possibility for human drug-drug interaction.

DY-9760e, 3-[2-[4-(3-chloro-2-methylphenyl)-1-piperazinyl]ethyl]-5,6-dimethoxy-1-(4-imidazolyl methyl)-1*H*-indazole dihydrochloride 3.5 hydrate (Fig. 1), is a novel calmodulin antagonist being developed to treat acute ischemic stroke. It inhibits calmodulin-dependent enzymes and in so doing exerts neuroprotective effects in animals with induced strokes (Sugimura et al., 1997; Sato et al., 1999, 2003, 2004; Fukunaga et al., 2000; Takagi et al., 2001; Hashiguchi et al., 2003). In an experimental model rats with transient focal ischemia, DY-9760e significantly reduces the infarct volume when infused for 6 h from 1 h after the middle cerebral artery occlusion, and also suppresses the increase in brain water content. Results of a previous study show that DY-9760e is metabolized by human liver microsomes in vitro, and the major metabolites of DY-9760e are identified as *N*-dealkylated (DY-9836), 4-hydroxylated (M3), *O*-demethylated (M5 and M7), and imidazole oxidized derivatives (M6 and M8) (Fig. 1; Tachibana et al., 2005b). The results of pharmacokinetic studies in rats after intravenous administration of DY-9760e show that DY-9760e is extensively metabolized in the liver, and most of the administered DY-9760e is excreted into bile as glucuronide conjugates of hydroxylated and *O*-demethylated metabolites (Tachibana et al., 2005a). Therefore, DY-9760e is eliminated mainly through hepatic metabolic clearance.

Although the general outline of DY-9760e metabolism is known, more specific information is needed to understand its complex metabolism. Thus, this study had 2 purposes. One purpose of this study was to identify which human CYP isozyme(s) are involved in the formation of the primary metabolites of DY-9760e, and to determine the enzyme kinetics for the formation of metabolites using human liver microsomes and

microsomes expressing recombinant human CYP enzymes. These studies provide essential information for determining the contribution of each CYP isozyme to DY-9760e metabolism. The second purpose of the present study was to estimate how potently DY-9760e inhibits CYP enzymes in vitro. DY-9760e bears an imidazole ring in its structure. Results of several previous studies have shown that some compounds containing the imidazole ring, such as ketoconazole, itraconazole, and miconazole, are potent inhibitors of CYP3A4 and 2C9 (Wilkinson et al., 1974; Rogerson et al., 1977; Ahmed et al., 1995; Halpert, 1995; Venkatakrishnan et al., 2000). In order to use DY-9760e safely and predict possible drug-drug interactions in humans, the inhibitory effects of DY-9760e against CYP1A2-, 2C9-, 2C19-, 2D6-, 2E1-, and 3A4-catalyzed metabolic reactions were investigated in vitro using human liver microsomes.

Materials and Methods

Chemicals. DY-9760e, DY-9836 (an *N*-dealkylated derivative), D91-6505a (M5), D91-4389a (M3), and DX-9194 used as an internal standard for LC-MS analysis were synthesized by Daiichi Pharmaceutical Co., Ltd. (Tokyo, Japan). Glucose-6-phosphate (G-6-P), glucose-6-phosphate dehydrogenase (G-6-PDH), and β-NADPH were purchased from Oriental Yeast Co., Ltd. (Tokyo, Japan). 7-Ethoxyresorufin and resorufin sodium, were purchased from Sigma Chemical Co. (St. Louis, MO, USA); tolbutamide was from Wako Pure Chemical Industries, Ltd. (Osaka, Japan); and 4-hydroxytolbutamide, *(S)*-mephenytoin, 4'-hydroxymephenytoin, bufuralol hydrochloride, midazolam hydrochloride, and 1'-hydroxymidazolam were purchased from Daiichi Pure Chemicals Co., Ltd. (Tokyo, Japan). All other chemical reagents were analytical grade.

Microsomes and antiserum. Human liver microsomes (pool of 16 donors: 0.432 nmol P450/mg protein) were purchased from XenoTech LLC (Kansas City, KS, USA). In kinetic analysis experiments, human liver microsomes (pool of 11 donors, 0.550 nmol P450/mg protein) obtained from Gentest Corp. (Woburn, MA, USA) were used. A bank of fully characterized human liver microsomes from 16 different donors (Reaction Phenotyping Kit) purchased from XenoTech LLC was used in correlation analysis experiments. Microsomes prepared from insect cells transfected with a baculovirus co-expressing one of the following recombinant human CYP enzymes (CYP1A1, 1A2, 2A6, 2B6, 2C8, 2C9*1 [Arg144]+cytochrome b_5 [thereafter b_5], 2C9*2 [Cys144], 2C18, 2C19, 2D6*1, 2E1+b_5, 3A4, 3A4+b_5, 3A5, and 4A11) and human NADPH-cytochrome P450 reductase (Supersomes™) were obtained from Gentest Corp.

Anti-human CYP polyclonal rabbit antiserum (anti-human CYP1A1, 1A1/2, 2A6, 2C8, 2C9, 2C19, 2D6, 2E1, and 3A4) were purchased from Nihon Nosan Kogyo K.K. (Yokohama, Japan). Non-immune rabbit serum was obtained from Gibco BRL (Grand Island, NY, USA).

Microsomal incubations. Each reaction mixture consisted of 50 mM Tris-HCl buffer (pH 7.4), 0.25 mg/ml human liver microsomes, DY-9760e dissolved in methanol (1%, v/v), 12 mM G-6-P, 2.2 units/ml G-6-PDH, 5 mM $MgCl_2$, and 1 mM NADPH in a total volume of 400 µl. An initial experiment was conducted to find the optimal microsomal protein concentration and incubation time that resulted in a linear reaction velocity. After a 5-min pre-incubation period at 37°C, the reactions were started by the addition of NADPH and carried out at 37°C for 10 min. The reactions were terminated by adding 1 ml of acetonitrile, after which 100 µl of the internal standard solution (2 µg/ml DX-9194) was added. After centrifugation at 1500*g* for 10 min, each supernatant was evaporated to dryness and dissolved in 400 µl of a 60:40 (v/v) mixture of 10 mM ammonium acetate (adjusted to pH 7.4) and acetonitrile. A 20-µl aliquot of each reconstituted mixuture was separately loaded onto the LC-MS system as described in the “Analytical procedure” section. Since chemically synthetic compounds of M6, M7, and M8 were not available, the concentration of M7 was calculated using the calibration curve for its isomer, D91-6505a (M5), and the concentrations of M6 and M8 were calculated from the calibration curve for DY-9836.

Immunoinhibition study. Pooled human liver microsomes (0.25 mg/ml), anti-human CYP polyclonal antiserum diluted with non-immune rabbit serum, and 50 mM Tris-HCl buffer (pH 7.4) were combined and incubated for 10 min at room temperature. A reaction mixture containing 10 µM DY-9760e was added and

pre-incubated for 5 min at 37˚C. The reactions were started by adding 1 mM NADPH, and each reaction was allowed to proceed for 10 min at 37ºC.

Correlation analysis with a panel of human liver microsomes. DY-9760e (6.3 μM) was incubated with a bank of characterized human liver microsomes (0.5 mg/ml). Reaction velocities for the formation of the DY-9760e metabolites were correlated against the marker activities specific for each CYP isozyme in the same microsomal reaction mixtures. The CYP-specific marker activities of the individual microsomes were described in the data sheet provided by the manufacturer. Pearson's correlation coefficient and corresponding *p* values for the correlation were used to assess the relationship between the CYP marker activities and the formation rates of DY-9760e metabolites. The two-tailed statistically significant difference was set at a *p*-value of 0.05. Statistical analysis was performed using EXSAS ver. 5.00 (Arm Corp.; Osaka, Japan) based on SAS release 6.12 (SAS Institute Japan; Tokyo, Japan).

Reactions with recombinant human CYP enzymes (Initial screen test). DY-9760e at two concentrations, 6.3 or 50 μM, was incubated with a set of 15 recombinant human CYP-expressing microsomes (Supersomes™) in 400 μl volume reaction mixtures. After a 2-min warming period at 37˚C, the reaction was started by the addition of ice-cold microsomes (50 pmol CYP) and the reaction was conducted for 30 min at 37ºC.

Analytical procedure. LC-MS in selected ion monitoring (SIM) mode was used to analyze the DY-9760e metabolites in the microsomal reaction mixtures. The instruments used for LC-APCI-MS were a Finnigan LCQ ion trap mass spectrometer (Thermo Electron Corporation; San Jose, CA, USA) equipped with an Alliance 2690 HPLC system (Waters Corp.; Milford, CA, USA). Chromatographic separation of

metabolites was carried out on a Symmetry C18 column (5 μm; 150 mm × 4.6 mm I.D.; Waters Corp.) at 40°C. A linear gradient of 30% to 60% acetonitrile in 10 mM ammonium acetate (adjusted to pH 7.4) over 30 min was used as the column eluent at a flow rate of 1 ml/min. The entire 1 ml/min flow was directed into the source of the mass spectrometer without splitting. APCI conditions in positive mode on the ion trap mass spectrometer were as follows: discharge voltage; 5.5 kV, discharge current; 5 μA, vaporizer temperature; 450°C, capillary voltage; 3 V, capillary temperature; 200°C, tube lens voltage; 20 V, and sheath gas (N_2); 80 arbitrary units.

Enzyme kinetics by human liver microsomes or recombinant CYP enzymes. The enzyme kinetics of DY-9760e metabolism by pooled human liver microsomes and 7 recombinant human CYP enzymes (CYP1A1, 1A2, 2C8, 2C9+b_5, 2C19, 2D6, and 3A4+b_5) was investigated at the concentrations of DY-9760e ranged from 0.4 to 500 μM. Formation of all the metabolites by 50 pmol of recombinant CYP enzymes was linear over time to 10 min, therefore, incubations were conducted for this time period. Both [V/S]-[V] plots (Eadie-Hofstee plot) and [S]-[V] plots were used to analyze the kinetic data. Appropriate enzyme kinetics models to define the substrate concentration-velocity functions were determined from the Eadie-Hofstee plots. The data were fitted to various enzyme kinetics models using the GraFit 5.0 software (Erithacus Software Ltd.; Horley, UK), designed for nonlinear regression analysis. The kinetic parameters were calculated after finding the model that best fit the data from among the following five equations:

the single-site Michaelis-Menten model

$$v = V_{max} \bullet [S] / (K_m + [S]) \quad (1)$$

the two-site Michaelis-Menten model

DMD Fast Forward. Published on July 27, 2005 as DOI: 10.1124/dmd.105.004903
This article has not been copyedited and formatted. The final version may differ from this version.

$$v = V_{max1} \cdot [S] / (K_{m1} + [S]) + V_{max2} \cdot [S] / (K_{m2} + [S]) \quad (2)$$

the modified two-site Michaelis-Menten model (biphasic model; Clarke, 1998)

$$v = (V_{max1} \cdot [S] + CL_{int,\ low\ affinity} \cdot [S]^2) / (K_{m1} + [S]) \quad (3)$$

if $[S] >> K_{m1}$ in equation (3),

$$v = V_{max1} \cdot [S] / (K_{m1} + [S]) + CL_{int,\ low\ affinity} \cdot [S] \quad (3')$$

the substrate inhibition model

$$v = V_{max} \cdot [S] / (K_m + [S] + [S]^2 / K_s) \quad (4)$$

K_s: substrate inhibition constant

and the autoactivation model (Hill equation).

$$v = V_{max} \cdot [S]^n / (K_m + [S]^n) \quad (5)$$

n: Hill coefficient

Inhibition of CYP enzymes by DY-9760e. To determine the effects of DY-9760e on each CYP isozyme, CYP isozyme-specific substrates were incubated at 37˚C with human liver microsomes in the presence or absence of varying concentrations of DY-9760e. Metabolic activities specific for each CYP isozyme were as follows: 7-ethoxyresorufin *O*-deethylation for CYP1A2 (Leclercq et al., 1996), tolbutamide 4-methylhydroxylation for CYP2C8/9 (Chen et al., 1993), (*S*)-mephenytoin 4'-hydroxylation for CYP2C19 (Meier et al., 1985), bufuralol 1'-hydroxylation for CYP2D6 (Kronbach et al., 1987), chlorzoxazone 6-hydroxylation for CYP2E1 (Peter et al., 1990), and midazolam 1'-hydroxylationfor CYP3A4 (Kronbach et al., 1989). These activities were determined using published methods after some modification. The amount of metabolite produced in each reaction mixture was analyzed by HPLC. Instruments used for HPLC were controlled by Hitachi D-7000 system manager (Hitachi, Ltd.; Tokyo, Japan) and consisted of an L-7100 pump, an L-7610 degasser, an

L-7300 column oven, an L-7200 autosampler, an L-7455 UV detector, and an L-7480 fluorescence detector. Lineweaver-Burk plots (L-B plot) were used to analyze the mechanism of inhibition, and K_i values were determined by Dixon plots. When the inhibitory mechanism was found to be a mixed type of competitive and non-competitive inhibitions, both K_i and K_I values were determined. K_I represents the dissociation constant of the interaction between the enzyme-substrate complex and inhibitor. For K_I determination, the *y*-intercept of the L-B plot was plotted against inhibitor concentration, and the intercept on the *x*-axis of a linear regression line was obtained ([I] vs. *y*-intercept of L-B plot) (Palmer, 1991).

DMD Fast Forward. Published on July 27, 2005 as DOI: 10.1124/dmd.105.004903
This article has not been copyedited and formatted. The final version may differ from this version.

Results

Enzyme kinetic studies using human liver microsomes. The [*S*]-[*V*] plots for the formation of each DY-9760e metabolite by human liver microsomes are shown in Fig. 2, and the kinetics values are shown in Table 1. Kinetic analysis revealed that the formation rates of M3, M5, M6, M7, and DY-9836 by human liver microsomes were not consistent with a Michaelis-Menten kinetics model, but were better described by a substrate inhibition model (equation 4). The formation of M3, M5, and M6 could not be completely fitted to the substrate inhibition model over a wide range of DY-9760e concentrations from 0.4 to 500 μM. Therefore, taking human plasma level of DY-9760e into consideration, the data for DY-9760e concentrations greater than 200 or 500 μM were excluded from the nonlinear regression analysis to obtain the best fit at low substrate concentrations. In contrast, the formation rate of M8 was consistent with a single-enzyme Michaelis-Menten model over the entire substrate concentration range (equation 1).

The K_m values of all metabolites were similar ranging between 1.2 and 3.6 μM. These values suggest a high affinity of the metabolic enzymes for DY-9760e. The substrate inhibition constant K_s was ranged from 197 to 1713 μM; as a consequence DY-9760e is thought to have little inhibitory effect on its own metabolism in vivo at the clinically effective dose.

Immunoinhibition. The inhibitory effects of rabbit anti-human CYP antiserum on DY-9760e metabolism are shown in Fig. 3. Anti-human CYP1A1/2, 2A6, 2D6, and 2E1 antiserum had no inhibitory effects (data not shown). The formation of M3, M6, M7, M8, and DY-9836 were strongly inhibited by anti-CYP3A4 antiserum in a concentration-dependent manner. However, the formation of M5 was not inhibited by

anti-CYP3A4 antiserum. Instead, anti-CYP2C9 antiserum concentration-dependently inhibited the formation of M5. Although anti-CYP1A1, 2C8, and 2C19 antiserum also inhibited the formation of M5, this inhibition was relatively weak (50%–70% of control activity remaining).

Correlation studies. The correlation coefficients between the activities of each DY-9760e metabolite formation and the substrate specific for each CYP tested in a bank of characterized human liver microsomes are summarized in Table 2. The formation rates of M3, M6, M7, M8, and DY-9836 varied over a 7-fold range, and the rates for these metabolites correlated significantly (r = 0.947 – 0.973; p < 0.001) with CYP3A4/5-selective testosterone 6β-hydroxylation activity at a DY-9760e concentration of 6.3 μM. A significant correlation with paclitaxel 6α-hydroxylation activity catalyzed by CYP2C8 was also observed for the formation of M3, M7, M8, and DY-9836, but was relatively weak (r = 0.503 – 0.682). The formation rate of M5 had a 3-fold sample-to-sample variation and correlated significantly with the diclofenac 4'-hydroxylation catalyzed by CYP2C9 (r = 0.860 ; p < 0.001).

Enzyme kinetic studies using human recombinant CYP enzymes. From the results of the initial screen with 15 different recombinant human CYP enzymes, CYP3A4 activity in the presence of b_5 for the formation of M3, M6, M7, M8, and DY-9836 was much higher than any other CYP enzymes examined, and the formation of M5 was catalyzed by recombinant CYP2C9, 2C19, and 2D6 (data not shown). In addition to these CYP enzymes, CYP1A1, 1A2, and 2C8 possess relatively high DY-9760e metabolic activities; therefore, enzyme kinetics values for metabolite formation by these 7 recombinant human CYP enzymes were obtained. The [S]-[V] plots for the formation of each metabolite by recombinant CYP3A4+b_5 are shown in Fig.

4, and all kinetics values are shown in Table 3.

Most data sets fit one of the Michaelis-Menten models (equations 1 and 2), but there were several data sets that could not be fit to the classical hyperbolic curve in [*S*]-[*V*] plots. These data sets represented convex or sigmoidal curves that resulted from substrate inhibition (equation 4) and autoactivation (equation 5), respectively. Substrate inhibition and autoactivation kinetics were also discernible from characteristic curved lines in Eadie-Hofstee plots, which are useful diagnostic plots for identifying a suitable kinetic model. Kinetics data for M3 formation by CYP1A1 and 2C8, M5 formation by CYP2C9 and 2C19, and DY-9836 formation by CYP2C19 represented convex curves, which fit a substrate inhibition model. In contrast, the enzyme kinetics for all metabolites formed by CYP3A4 was described by a sigmoidal curve with autoactivation and fit a Hill model (equation 5, Fig. 4). Eadie-Hofstee plots also exhibited curved lines characteristic of autoactivation (inset graphs in Fig. 4). For the formation of M5 by CYP3A4, the rates best fit the following equation, derived simply by combining equations (3') and (5) (Fig. 4).

$$v = V_{max} \bullet [S]^n / (K_m + [S]^n) + CL_{int,\ low\ affinity} \bullet [S] \qquad (9)$$

For the formation of M3 and M6 by CYP3A4, the [*S*]-[*V*] plots showed sigmoidal curves at low substrate concentrations (≤50 μM), but rates decreased as substrate concentrations increased (inset graphs in Fig. 4). These results suggest that both autoactivation and substrate inhibition occur in one metabolic reaction, but no single model best describes these reactions. Therefore, curve fitting was carried out after excluding the data points for concentrations greater than 100 μM, because therapeutic plasma concentrations of DY-9760e are thought to rarely exceed 50 μM. Further analysis also revealed that the rate of CYP2C8-catalyzed M5 formation fits a biphasic

DMD Fast Forward. Published on July 27, 2005 as DOI: 10.1124/dmd.105.004903
This article has not been copyedited and formatted. The final version may differ from this version.

model using equation (3).

The enzyme kinetics analysis revealed the following information: (1) For the formation of M3, M6, M8 and DY-9836, CYP3A4 showed higher V_{max}/K_m values than any other CYP enzymes. (2) CYP2C9, 2C19, and 2D6 showed low K_m (<1.0 μM) and high V_{max} values for the formation of M5. (3) For the formation of M7, CYP2C19 and 2D6 showed higher V_{max}/K_m values than CYP3A4, resulting from their high substrate affinity, $K_m \leq 0.6$ μM. However, the V_{max} values of these CYPs are very low (≤22 pmol/min/nmol CYP). In contrast, CYP3A4 also showed a high capacity, with a V_{max} of 308.5 pmol/min/nmol CYP but with a moderate affinity of K_m = 14.6 μM. (4) For the formation of M3, CYP2C8 also showed a high catalytic activity of 118.2 μL/min/nmol CYP, the same activity as CYP3A4 (129.9 μL/min/nmol CYP). However, the V_{max} value of CYP3A4 was 3-fold higher than that of CYP2C8.

Inhibition of CYP enzymes by DY-9760e. Before each CYP inhibition study, preliminary experiments were conducted using a single substrate concentration around its K_m value and 1, 10, and 100 μM of DY-9760e. The result shows that DY-9760e is a potent inhibitor of CYP2C19, 2C9, and 2D6, and a moderate inhibitor of CYP3A4 and 1A2, with little effect on the CYP2E1 activity (data not shown). Using these preliminary data, appropriate substrate and inhibitor concentrations were selected for the determination of a precise inhibition constant (K_i value) for 5 different CYP isozyme-specific activities in human liver microsomes. K_i values were determined from Dixon plots as shown in Fig. 5. DY-9760e showes strong inhibitory effects on tolbutamide 4-methylhydroxylation catalyzed by CYP2C8/9 (K_i = 1.7 μM), (*S*)-mephenytoin 4'-hydroxylation catalyzed by CYP2C19 (K_i = 2.5 μM), and bufuralol 1'-hydroxylation catalyzed by CYP2D6 (K_i = 0.25 μM). The effects of DY-9760e on

DMD Fast Forward. Published on July 27, 2005 as DOI: 10.1124/dmd.105.004903
This article has not been copyedited and formatted. The final version may differ from this version.

7-ethoxyresorufin *O*-deethylation catalyzed by CYP1A2 (K_i = 22.2 μM), midazolam 1'-hydroxylation (K_i = 11.7 μM) catalyzed by CYP3A4 are moderate. The mechanisms of inhibition of DY-9760e, judging from the L-B plots, are competitive for CYP1A2, 2C8/9, 2D6, and 3A4. As for CYP2C19, the L-B plots for each DY-9760e concentration showed a common intercept left of the y-axis and above the x-axis, indicating a mixed competitive and non-competitive inhibition mechanism. The K_I value was 9.3 μM, as determined from the secondary plot ([I] vs. y-intercept of L-B plot) shown in Fig. 5F.

Discussion

Results of pharmacokinetics studies in rats and monkeys revealed that DY-9760e is eliminated mainly through hepatic metabolic clearance (Tachibana et al., 2005a). Furthermore, a Phase I pharmacokinetics study in healthy men revealed that the fraction of the dose excreted in the urine as unchanged DY-9760e is low, accounting for less than 1.5% of the administered dose (Daiichi Pharmaceutical, data on file). Although the full in vivo metabolic profile of DY-9760e in humans has not yet been identified, results from an in vitro metabolic study using human liver microsomes show that DY-9760e is extensively metabolized (Tachibana et al., 2005b). Therefore, in the present study, the CYP isozymes involved in the formation of the metabolites by human liver microsomes were identified.

The results from the immunoinhibition study (Fig. 3) and CYP activity correlation study (Table 2) suggest that CYP3A4 is responsible for majority of DY-9760e metabolism, with the exception of the formation of M5 (5-demethylated derivative), which is mainly catalyzed by CYP2C9. However, reactions of DY-9760e with recombinant human CYP enzymes revealed that other CYP isozyme can also metabolize DY-9760e. Enzyme kinetic analysis using human liver microsomes (Table 1) and recombinant CYP enzymes (Table 3) yielded much information on the contribution of CYP enzymes to DY-9760e metabolism. A substrate inhibition or Michaelis-Menten kinetics model results in the best fitting for the formation of all DY-9760e metabolites in human liver microsomes (Fig. 2), whereas autoactivation, which is observed by recombinant CYP3A4 (Fig. 4), does not occur. This might have resulted from the contribution of CYP isozymes other than CYP3A4 at low substrate concentrations in human liver microsomes. Moreover, kinetics of the formation of M3, M5, and M6 in

human liver microsomes is unique; substrate inhibition occurs at the concentrations of 25–200 μM, but the reaction velocity increases again at concentrations greater than 100–200 μM. These kinetic profiles derived from human liver microsomes might not reflect a reaction of a single enzyme, but combined reactions by more than one enzyme. As shown in Table 3, for the formation of M3, CYP2C8 possess a high catalytic activity (V_{max}/K_m) equal to CYP3A4 activity, and the K_m value of recombinant CYP2C8 is lower than that of CYP3A4. The correlation coefficient for the M3 formation with CYP2C8-selective activity (Table 2) was statistically significant, although it was relatively weak (r = 0.682). Therefore, in addition to CYP3A4, CYP2C8 makes some contribution to the formation of M3 at low substrate concentrations. For the formation of M5, CYP2C9 mainly catalyzes this reaction, but CYP2C19 showed higher V_{max}/K_m value and lower K_m value than those of CYP2C9. These results suggest that the contribution of CYP2C19 is not negligible at low substrate concentrations. CYP2D6 can catalyze the formation of M5, however, its contribution would be only minor because of low relative abundance in the liver.

The contributions of specific CYP enzymes to the total metabolic clearance can be estimated from their relative abundance in the liver or relative activity factors (RAF) (Crespi, 1995) during in vitro studies. Determining the contribution of each CYP isozyme at various substrate concentrations will be important to understand the complicated metabolic reaction. According to the RAF approach, the contribution of each CYP to DY-9760e metabolite formation in human liver microsomes was estimated, and the results confirmed the contribution of CYP2C8 for the M3 formation and CYP2C19 for the M5 formation at clinically relevant concentrations (about 2 μM) (data not shown).

DMD Fast Forward. Published on July 27, 2005 as DOI: 10.1124/dmd.105.004903
This article has not been copyedited and formatted. The final version may differ from this version.

For the last several years, a large number of examples of atypical enzyme kinetics have been observed in drug metabolism reactions (Ekins et al., 1998; Houston and Kenworthy, 2000; Kenworthy et al., 2001; Shou et al., 2001; Hutzler and Tracy 2002; Tracy 2003; Atkins, 2004). In order to avoid mis-estimation of kinetic parameters, it is necessary to apply an appropriate kinetic model to the in vitro data, especially when extrapolating in vitro findings to the in vivo conditions. Three kinds of atypical kinetic models (autoactivation, substrate inhibition, and biphasic) are needed to explain the metabolism of DY-9760e. Interestingly, the kinetics for M5 formation by CYP3A4 was best described by a mixed model of autoactivation and biphasic kinetics (Fig. 4). A non-exhaustive literature search suggests that this is the first example of a combination model with autoactivation kinetics by the CYP3A4 enzyme. However, it must be noted that the catalytic activity of CYP3A4 in vitro system can be influenced by various incubation conditions. The atypical kinetics of DY-9760e metabolism by CYP3A4 are observed in the presence of b_5 and magnesium, both which have been shown to influence the CYP3A4 activity (Guengerich et al, 1986; Yamazaki et al., 1995). Maenpaa et al. (1998) have reported that the buffer conditions, ionic strength, and the source of reducing agents affected the midazolam hydroxylation activity. Furthermore, the kinetics of the oxidation of pyrene by CYP3A4 is sigmoidal in the absence of magnesium but biphasic in the presence of magnesium (Schrag and Wienkers, 2000). Although it is difficult to determine the optimal conditions reflecting in vivo situations, further investigation will be needed using various incubation conditions.

It has been hypothesized that most atypical enzyme kinetics is caused by the simultaneous binding of more than one substrate molecule to an enzyme's active site, although several other hypotheses including an allosteric model have been proposed

DMD Fast Forward. Published on July 27, 2005 as DOI: 10.1124/dmd.105.004903
This article has not been copyedited and formatted. The final version may differ from this version.

(Ueng et al., 1997; Korzekwa et al., 1998). If the substrate binds to two or more sites, one of which triggers positive or negative cooperativity, the resulting kinetics might exhibit autoactivation or substrate inhibition, respectively. The formation rates of M3 and M6 by recombinant CYP3A4 can be fitted to an autoactivation model at <50 μM, but substrate inhibition subsequently occurred at >50 μM. If these results are correct, and not artifacts, DY-9760e is the substance to exert both positive and negative cooperativity on CYP3A4.

Fig. 5 shows that DY-9760e potently inhibits CYP2D6, 2C8/9, and 2C19 specific activities with low K_i values. The low K_i values for these CYP isozymes are a reflection of the low K_m values. In contrast, the inhibitory effects on CYP1A2 and 3A4 are relatively moderate, with K_i values of greater than 10 μM, although CYP3A4 is the major contributor to the metabolism of DY-9760e with high capacity. Kenworthy et al. (1999) have shown that more than one probe substrate should be used when estimating inhibitory constants for inhibitors of CYP3A4, because K_i values for inhibitors of CYP3A4 may be different depending on which probe substrate is being used. Therefore, the inhibitory effect on testosterone 6β-hydroxylation activity in addition to midazolam 1'-hydroxylation was tested using the method described previously (Tachibana and Tanaka, 2001). DY-9760e showed similar inhibitory effect on testosterone 6β-hydroxylation with K_i value of 15 μM (data not shown).

Compounds with chemically similar structures often show common characteristics as the inhibitors of CYP enzymes (Halpert, 1995; Ortiz de Montellano and Correia, 1995). DY-9760e contains both an imidazole ring, like ketoconazole and miconazole (CYP3A4 and 2C9 inhibitors), and methoxy groups such as quinidine (a CYP2D6 inhibitor). These chemical structures appear to contribute to the strong inhibitory effects

of DY-9760e on CYP enzymes. Further investigation will be needed concerning the relationship between the chemical structure of DY-9760e and its strong inhibitory effects on each CYP isozyme.

In clinical situations, the human plasma concentrations of DY-9760e will be kept under 1 μg/ml (about 2 μM), but the drug concentrations around metabolic enzymes in the liver would be higher than the plasma concentrations. The in vitro data from the present study demonstrated that DY-9760e at therapeutically relevant concentrations might be a strong inhibitor of CYP2C9, 2C19, and 2D6. Clinical investigations of DY-9760e with drugs that might be concomitantly administered are required to predict drug-drug interactions in humans. Since DY-9760e is intended for administration as a continuous infusion to treat the acute phase of cerebral ischemic damage, there will be few drugs taken simultaneously with DY-9760e. Nevertheless, it is possible that clinical use of DY-9760e would be limited.

In conclusion, CYP3A4 and 2C9 are significantly involved in DY-9760e metabolism in the human liver. In addition, CYP2C8 and 2C19 make minor contributions to DY-9760e metabolism. The kinetic profile of DY-9760e can be described by a non-Michaelis-Menten model, including substrate inhibition, autoactivation, and biphasic metabolism. DY-9760e appears to be a broad-spectrum inhibitor of the CYP enzymes; thus, clinically significant drug-drug interactions could occur between DY-9760e and substrates of CYP2C9, 2D6, and 2C19.

Acknowledgments.

The authors thank Mr. Steve E. Johnson for editing this manuscript.

References

Ahmed S, Smith JH, Nicholls PJ, Whomsley R and Cariuk P (1995) Synthesis and biological evaluation of imidazole based compounds as cytochrome P-450 inhibitors. *Drug Des Discov* **13:** 27–41.

Atkins WM (2004) Implications of the allosteric kinetics of cytochrome P450s. *Drug Discov Today* **9:** 478–484.

Chen LS, Yasumori T, Yamazoe Y, and Kato R (1993) Hepatic microsomal tolbutamide hydroxylation in Japanese: in vitro evidence for rapid and slow metabolizers. *Pharmacogenetics* **3**: 77–85.

Clarke SE (1998) In vitro assessment of human cytochrome P450. *Xenobiotica*. **28:**1167–1202.

Crespi CL (1995) Xenobiotic-metabolizing human cells as tools for pharmacological and toxicological research. *Adv Drug Res* **26:**179–235.

Ekins S, Ring BJ, Binkley SN, Hall SD and Wrighton SA (1998) Autoactivation and activation of the cytochrome P450s. *Int J Clin Pharmacol Ther* **36:**642–651.

Fukunaga K, Ohmitsu M, Miyamoto E, Sato T, Sugimura M, Uchida T and Shirasaki Y (2000) Inhibition of neuronal nitric oxide synthase activity by 3-[2-[4-(3-chloro-2-methylphenyl)-1-piperazinyl]ethyl]-5,6-dimethoxy-1-(4-imidazolyl methyl)-1*H*-indazole dihydrochloride 3.5 hydrate (DY-9760e), a novel neuroprotective agent, in vitro and in cultured neuroblastoma cells in situ. *Biochem Pharmacol* **60:** 693–699.

Guengerich FP, Martin MV, Beaune PH, Kremers P, Wolff T and Waxman DJ (1986) Characterization of rat and human liver microsomal cytochrome P-450 forms involved in nifedipine oxidation, a prototype for genetic polymorphism in oxidative drug

metabolism. *J Biol Chem* **261:**5051–5060.

Halpert JR (1995) Structural basis of selective cytochrome P450 inhibition. *Annu Rev Pharmacol Toxicol* **35:** 29–53.

Hashiguchi A, Kawano T, Yano S, Morioka M, Hamada J, Sato T, Shirasaki Y, Ushio Y and Fukunaga K (2003) The neuroprotective effect of a novel calmodulin antagonist, 3-[2-[4-(3-chloro-2-methylphenyl)-1-piperazinyl]ethyl]-5,6-dimethoxy-1-(4-imidazolylmethyl)-1H-indazole dihydrochloride 3.5 hydrate,
in transient forebrain ischemia. *Neuroscience* **121:** 379–386.

Houston JB and Kenworthy KE (2000) In vitro-in vivo scaling of CYP kinetic data not consistent with the classical Michaelis-Menten model. *Drug Metab Dispos* **28**:246–254.

Hutzler JM and Tracy TS (2002) Atypical kinetic profiles in drug metabolism reactions. *Drug Metab Dispos* **30:** 355–362.

Kenworthy KE, Bloomer JC, Clarke SE and Houston JB (1999) CYP3A4 drug interactions: correlation of 10 in vitro probe substrates. *Br J Clin Pharmacol* **48:**716–727.

Kenworthy KE, Clarke SE, Andrews J and Houston JB (2001) Multisite kinetic models for CYP3A4: simultaneous activation and inhibition of diazepam and testosterone metabolism. *Drug Metab Dispos* **29:**1644–1651.

Korzekwa KR, Krishnamachary N, Shou M, Ogai A, Parise RA, Rettie AE, Gonzalez FJ and Tracy TS (1998) Evaluation of atypical cytochrome P450 kinetics with two-substrate models: evidence that multiple substrates can simultaneously bind to cytochrome P450 active sites. *Biochemistry* **37:**4137–4147.

Kronbach T, Mathys D, Gut J, Catin T, and Meyer UA (1987) High-performance liquid chromatographic assays for bufuralol 1'-hydroxylase, debrisoquine 4-hydroxylase, and

dextromethorphan O-demethylase in microsomes and purified cytochrome P-450 isozymes of human liver. *Anal Biochem* **162**: 24–32.

Kronbach T, Mathys D, Umeno M, Gonzalez FJ, and Meyer UA (1989) Oxidation of midazolam and triazolam by human liver cytochrome IIIA4. *Mol Pharmacol* **36**: 89–96.

Leclercq I, Desager JP, Vandenplas C, and Horsmans Y (1996) Fast determination of low-level cytochrome P-450 1A1 activity by high-performance liquid chromatography with fluorescence or visible absorbance detection. *J Chromatogr B* 681: 227–232.

Maenpaa J, Hall SD, Ring BJ, Strom SC and Wrighton SA (1998) Human cytochrome P450 3A (CYP3A) mediated midazolam metabolism: the effect of assay conditions and regioselective stimulation by alpha-naphthoflavone, terfenadine and testosterone. *Pharmacogenetics* **8:**137–155.

Meier UT, Kronbach T, and Meyer UA (1985) Assay of mephenytoin metabolism in human liver microsomes by high-performance liquid chromatography. *Anal Biochem* **151**: 286–291.

Ortiz de Montellano PR and Correia MA (1995) Inhibition of cytochrome P-450 enzymes, in *Cytochrome P-450: Structure, Mechanism and Biochemistry* (Ortiz de Montellano PR ed) pp 305–364, Plenum Press, New York.

Palmer T (1991) Enzyme inhibition, in *Understanding enzymes* (Palmer T. ed) pp139-164, Ellis Horwood, London.

Peter R, Böcker R, Beaune PH, Iwasaki M, Guengerich FP, and Yang CS (1990) Hydroxylation of chlorzoxazone as a specific probe for human liver cytochrome P-450IIE1. *Chem Res Toxicol* **3**: 566–573.

Rogerson TD, Wilkinson CF and Hetarski K (1977) Steric factors in the inhibitory interaction of imidazoles with microsomal enzymes. *Biochem Pharmacol* **26:**

1039–1042.

Sato T, Morishima Y, Sugimura M, Uchida T and Shirasaki Y (1999) DY-9760e, a novel calmodulin antagonist, reduces brain damage induced by transient focal cerebral ischemia. *Eur J Pharmacol* **370:** 117–123.

Sato T, Morishima Y and Shirasaki Y (2003) 3-[2-[4-(3-chloro-2-methylphenyl)-1-piperazinyl]ethyl]-5,6-dimethoxy-1-(4-imidazolyl methyl)-1H-indazole dihydrochloride 3.5 hydrate (DY-9760e), a novel calmodulin antagonist, reduces brain edema through the inhibition of enhanced blood-brain barrier permeability after transient focal ischemia. *J Pharmacol Exp Ther* **304:** 1042–1047.

Sato T, Takamori H and Shirasaki Y (2004) DY-9760e, a novel calmodulin antagonist, reduces infarction after permanent focal cerebral ischemia in rats. *Pharmacology* **71:** 38–45.

Schrag ML and Wienkers LC (2000) Topological alteration of the CYP3A4 active site by the divalent cations Mg^{2+}. *Drug Metab Dispos* **28:**1198–1201.

Shou M, Lin Y, Lu P, Tang C, Mei Q, Cui D, Tang W, Ngui JS, Lin CC, Singh R, Wong BK, Yergey JA, Lin JH, Pearson PG, Baillie TA, Rodrigues AD and Rushmore TH (2001) Enzyme kinetics of cytochrome P450-mediated reactions. *Curr Drug Metab* **2:**17–36.

Sugimura M, Sato T, Nakayama W, Morishima Y, Fukunaga K, Omitsu M, Miyamoto E and Shirasaki Y (1997) DY-9760e, a novel calmodulin antagonist with cytoprotective action. *Eur J Pharmacol* **336:** 99–106.

Tachibana S and Tanaka M (2001) Simultaneous determination of testosterone metabolites in liver microsomes using column-switching semi-microcolumn high-performance liquid chromatography. *Anal Biochem* **295:**248-256.

Tachibana S, Fujimaki Y, Tachibana M, Tanaka M, Kurata T, Okazaki O and Sudo K (2005a) Pharmacokinetics and disposition of DY-9760e, a novel calmodulin antagonist, in rats and monkeys. *Arzneim-Forsch/Drug Res* **3:** 135-144.

Tachibana S, Tanaka M, Fujimaki Y, Suzuki W, Ookuma T, Ohori Y, Hayashi K, Iwata H, Okazaki O and Sudo K (2005b) Metabolism of the novel calmodulin antagonist DY-9760e, in animals and humans. *Xenobiotica* **35:** 499-517.

Takagi K, Sato T, Shirasaki Y, Narita K, Tamura A and Sano K (2001) Post-ischemic administration of DY-9760e, a novel calmodulin antagonist, reduced infarct volume in the permanent focal ischemia model of spontaneously hypertensive rat. *Neurol Res* **23:** 662–668.

Tracy TS (2003) Atypical enzyme kinetics: their effect on in vitro-in vivo pharmacokinetic predictions and drug interactions. *Curr Drug Metab* **4:**341-346.

Ueng YF, Kuwabara T, Chun YJ and Guengerich FP (1997) Cooperativity in oxidations catalyzed by cytochrome P450 3A4. *Biochemistry* **36:**370–381.

Venkatakrishnan K, von Moltke LL and Greenblatt DJ (2000) Effects of the antifungal agents on oxidative drug metabolism: clinical relevance. *Clin Pharmacokinet* **38:**111-180.

Wilkinson CF, Hetnarski K, Cantwell GP and DiCarlo FJ (1974) Structure-activity relationships in the effects of 1-alkylimidazoles on microsomal oxidation in vitro and in vivo. *Biochem Pharmacol* **23:** 2377–2386.

Yamazaki H, Ueng YF, Shimada T and Guengerich FP (1995) Roles of divalent metal ions in oxidations catalyzed by recombinant cytochrome P450 3A4 and replacement of NADPH--cytochrome P450 reductase with other flavoproteins, ferredoxin, and oxygen surrogates. *Biochemistry* **34:**8380–8389.

Footnotes

Address correspondence to: Shuko Tachibana; Drug Metabolism & Physicochemistry Research Laboratories, R&D Division, Daiichi Pharmaceutical Co., Ltd., 1-16-13, Kita-kasai, Edogawa-ku, Tokyo 134-8630, Japan.

Legends for figures:

FIG. 1. DY-9760e and its proposed major metabolic pathways in human liver microsomes from Tachibana et al. (2005b).

FIG. 2. The formation rates of M3, M5, M6, M7, M8, and DY-9836 by pooled human liver microsomes. Lines represent the best fit to either a substrate inhibition model (M3, M5, M6, M7, and DY-9836) or a single-enzyme Michaelis-Menten model (M8). Data points at 500 μM or 200 μM were excluded from the fitting lines in the plots of M3, M5, and M6. Insets: Eadie-Hofstee plots.

FiG. 3. Effects of anti-human CYP antiserum (■, anti-CYP1A1; ▲, anti-CYP2C8; ○, anti-CYP2C9; □, anti-CYP2C19; ●, anti-CYP3A4) on the formation of DY-9760e metabolites by human liver microsomes.

FIG. 4. The formation rates of M3, M5, M6, M7, M8, and DY-9836 by recombinant CYP3A4 + b_5 expressed in insect cell microsomes. Lines represent the best fit to an autoactivation model (M3, M6, M7, M8, and DY-9836) or a combined autoactivation−biphasic model (M5). Insets: Eadie-Hofstee plots.

FIG. 5. Dixon plots of the inhibition of (A) 7-ethoxyresorufin *O*-deethylation (CYP1A2 activity), (B) tolbutamide 4-methylhydroxylation (CYP2C8/9 activity), (C) *(S)*-mephenytoin 4'-hydroxylation (CYP2C19 activity), (D) bufuralol 1'-hydroxylation (CYP2D6 activity), and (E) midazolam 1'-hydroxylation (CYP3A4 activity) in human liver microsomes by DY-9760e. The secondary plot (F) was drawn by plotting the

y-intercept of L-B plot of the effect on *(S)*-mephenytoin 4'-hydroxylation (C) against DY-9760e concentration to estimate K_I value. Each point represents the mean of duplicate incubations. Lines represent results of linear regression of transformed data.

TABLE 1

Kinetics values for the metabolism of DY-9760e by human liver microsomes (0.550 nmol CYP/mg protein)

Metabolite	Pathway	K_m (μM)	V_{max} (pmol/min/mg protein)	V_{max} (pmol/min/nmol CYP)	V_{max}/K_m (μL/min/nmol CYP)	K_s (μM)	Kinetic model
M3	phenyl hydroxylation	1.6	67.6	122.9	76.8	284.6	substrate inhibition (<200 μM)
M5	5-demethylation	1.2	13.8	25.1	20.9	197.2	substrate inhibition (<100 μM)
M6	imidazole oxidation	2.5	59.8	108.7	43.5	256.4	substrate inhibition (<200 μM)
M7	6-demethylation	2.8	20.3	36.9	13.2	1713.3	substrate inhibition
M8	imidazole oxidation	2.8	105.9	192.5	68.8	-	Michaelis-Menten
DY-9836	*N*-dealkylation	3.6	69.8	126.9	35.3	1106.4	substrate inhibition

TABLE 2

Correlation of DY-9760e metabolism with specific CYP isozyme activity in human liver microsomes

CYP isozyme activity	CYP	Correlation coefficient (*r*)					
		M3	M5	M6	M7	M8	DY-9836
7-Ethoxyresorfin *O*-dealkylation	CYP1A2	0.003	-0.230	-0.067	0.078	0.009	0.020
Coumarin 7-hydroxylation	CYP2A6	0.218	0.465	0.206	0.124	0.194	0.137
(S)-Mephenytoin *N*-demethylation	CYP2B6	0.539*	0.472	0.412	0.443	0.438	0.420
Paclitaxel 6α-hydroxylation	CYP2C8	0.682**	0.364	0.377	0.522*	0.550*	0.503*
Diclofenac 4'-hydroxylation	CYP2C9	0.358	0.860***	0.219	0.245	0.309	0.231
(S)-Mephenytoin 4'-hydroxylation	CYP2C19	0.357	0.161	0.372	0.369	0.365	0.362
Dextromethorphan *O*-demethylation	CYP2D6	0.184	0.124	0.050	0.115	0.117	0.087
Chlorzoxazone 6-hydroxylation	CYP2E1	-0.015	0.211	-0.235	-0.181	-0.115	-0.161
Testosterone 6β-hydroxylation	CYP3A4/5	0.958***	0.215	0.947***	0.973***	0.957***	0.966***
Lauric acid 12-hydroxylation	CYP4A9/11	0.160	0.188	0.031	0.210	0.138	0.132

Formation of DY-9760 metabolites, M3, M5, M6, M7, M8, and DY-9836 were measured at 6.3 μM DY-9760e using a bank of characterized human liver microsomes from 16 individual donors (0.5 mg of protein/ml; 10-min incubation).
The correlations between DY-9760 metabolic activities with CYP isozyme marker activities were determined using EXSAS ver. 5.0.
*$p < 0.05$; **$p < 0.01$; ***$p < 0.001$.

TABLE 3

Kinetics values for the metabolism of DY-9760e by recombinant CYP microsomes

Metabolite (Pathway)	CYP	K_m (μM)	V_{max} (pmol/min/nmol CYP)	V_{max}/K_m (μL/min/nmol CYP)	V_{max2}/K_{m2} [a] (μL/min/nmol CYP)	K_s (μM)	*n* *Hill coefficient*	Kinetic model [b]
M3	1A1	1.1	16.7	15.2		438.3		SI (<50 μM)
(phenyl hydroxylation)	1A2	5.2	7.3	1.4	0.02			2-site M-M
	2C8	2.5	295.5	118.2		270.0		SI (weighted)
	2C9	1.2	8.6	7.2				M-M
	2C19	1.6	9.9	6.2				M-M
	2D6	0.7	19.7	30.3				M-M
	3A4	6.9	896.1	129.9			2.4	AA (<50 μM)
M5	2C8	3.1	12.8	4.2	0.08			Biphasic
(*O*-demethylation)	2C9	0.9	71.2	79.1		363.1		SI (<200 μM)
	2C19	0.5	72.9	145.8		315.4		SI (<200 μM)
	2D6	1.0	86.9	86.9				M-M
	3A4	11.9	29.9	2.5	0.10		2.1	AA + biphasic
M6	3A4	6.5	627.5	96.5			2.6	AA (<50 μM)
(imidazole oxidation)								
M7	2C19	0.3	16.2	54.5				M-M
(*O*-demethylation)	2D6	0.6	22.1	35.5				M-M
	3A4	14.6	308.5	21.1			1.8	AA
M8	1A1	1.1	198.85	153.6				M-M
(imidazole oxidation)	1A2	25.1	62.3	2.5				M-M
	2C8	2.6	73.2	28.2				M-M
	2C9	6.4	13.9	2.2	0.31			2-site M-M
	2C19	9.6	50.0	5.2				M-M
	2D6	1.4	147.8	105.6				M-M
	3A4	9.0	2167.5	240.8			2.0	AA
DY-9836	1A1	31.1	193.6	6.2				M-M
(*N*-dealkylation)	1A2	24.2	76.7	3.2				M-M
	2C8	15.2	23.1	1.5	0.25			2-site M-M
	2C9	54.2	51.2	0.9				M-M
	2C19	14.3	97.4	6.8		585.2		SI
	2D6	74.7	153.2	2.1				M-M
	3A4	7.1	1145.3	161.3			1.5	AA

[a] Low affinity site.
[b] SI: substrate inhibition; M-M: Michaelis-Menten; AA: autoactivation.

FIG.1

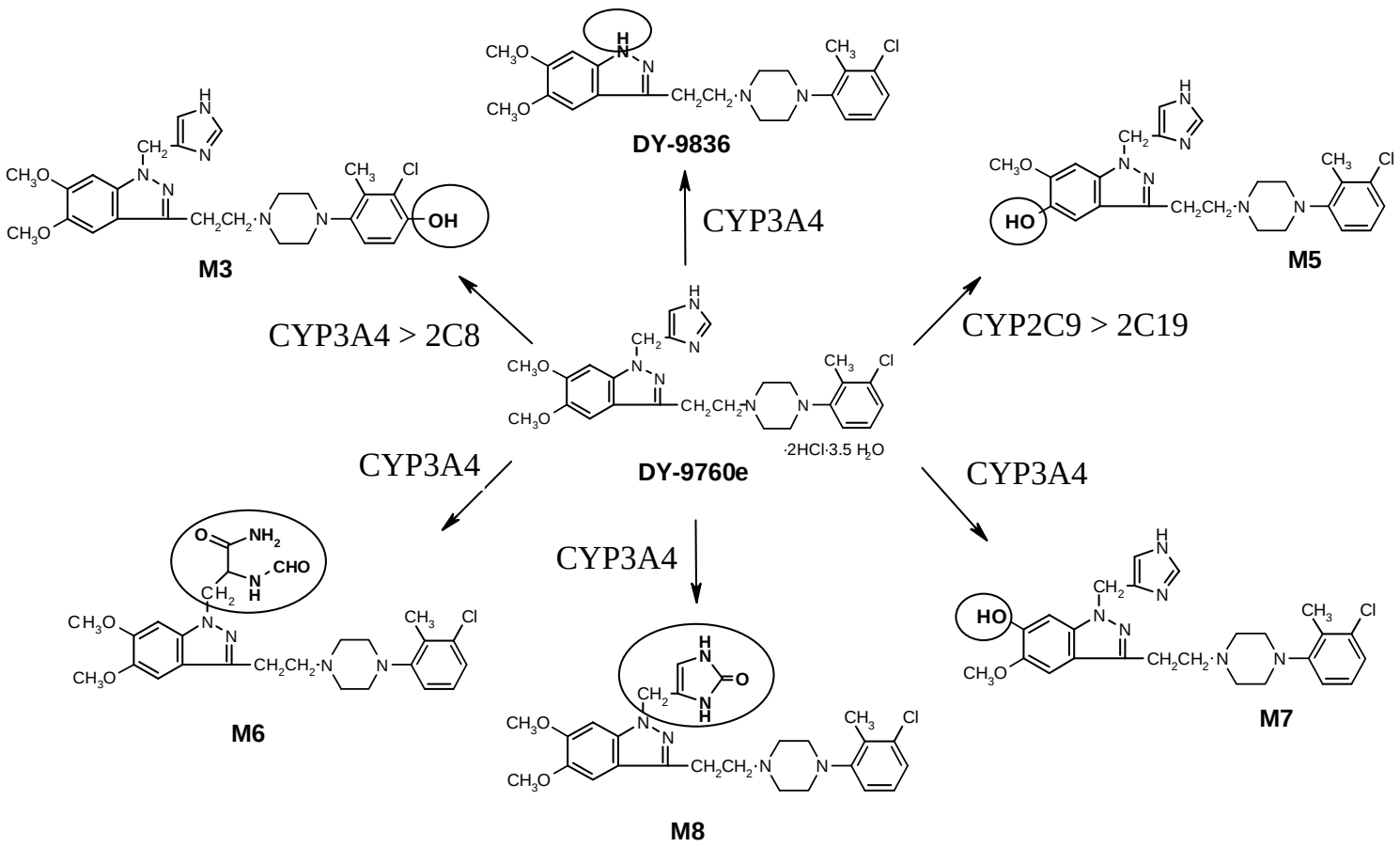

FIG.2

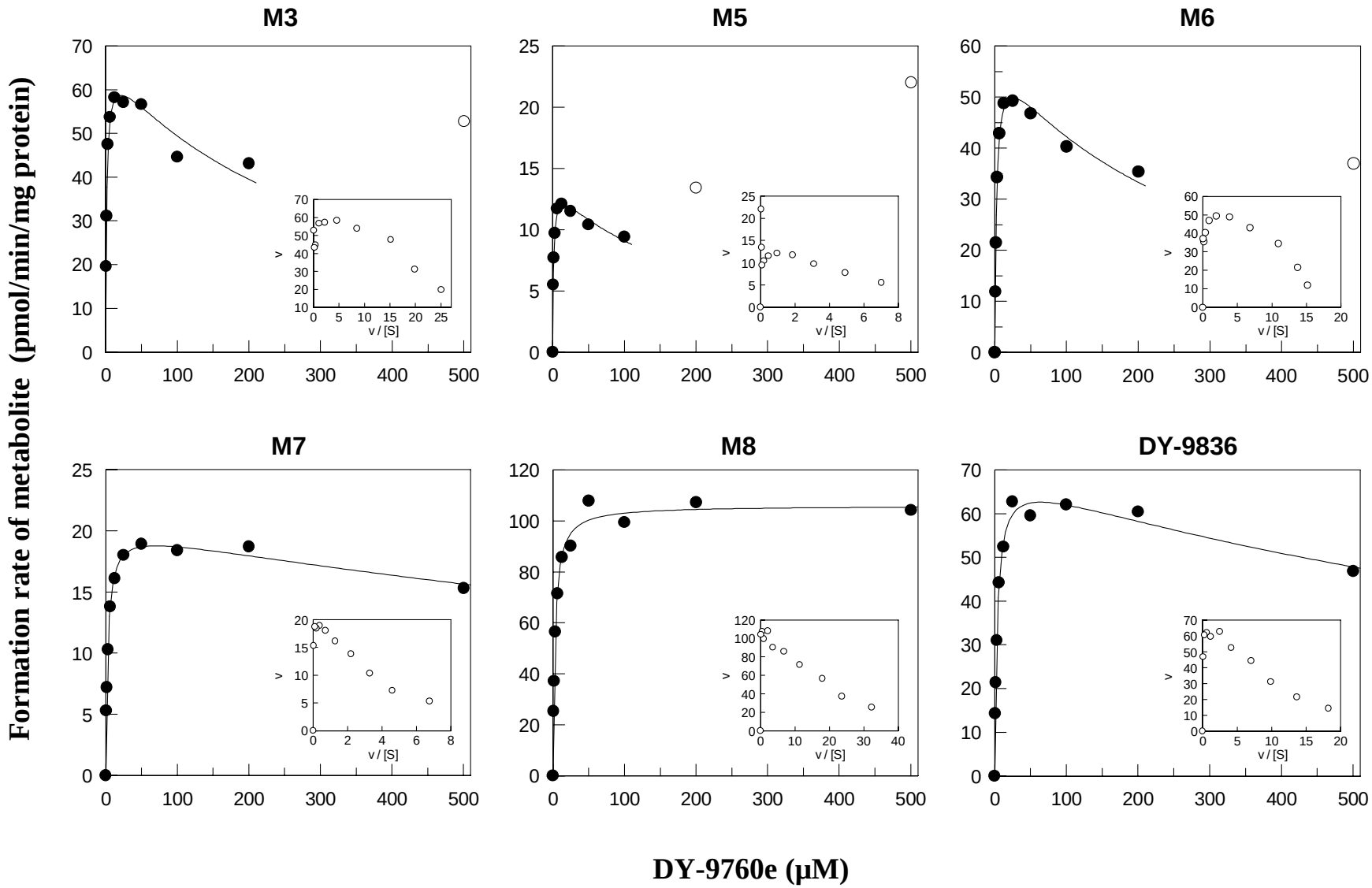

FIG.3

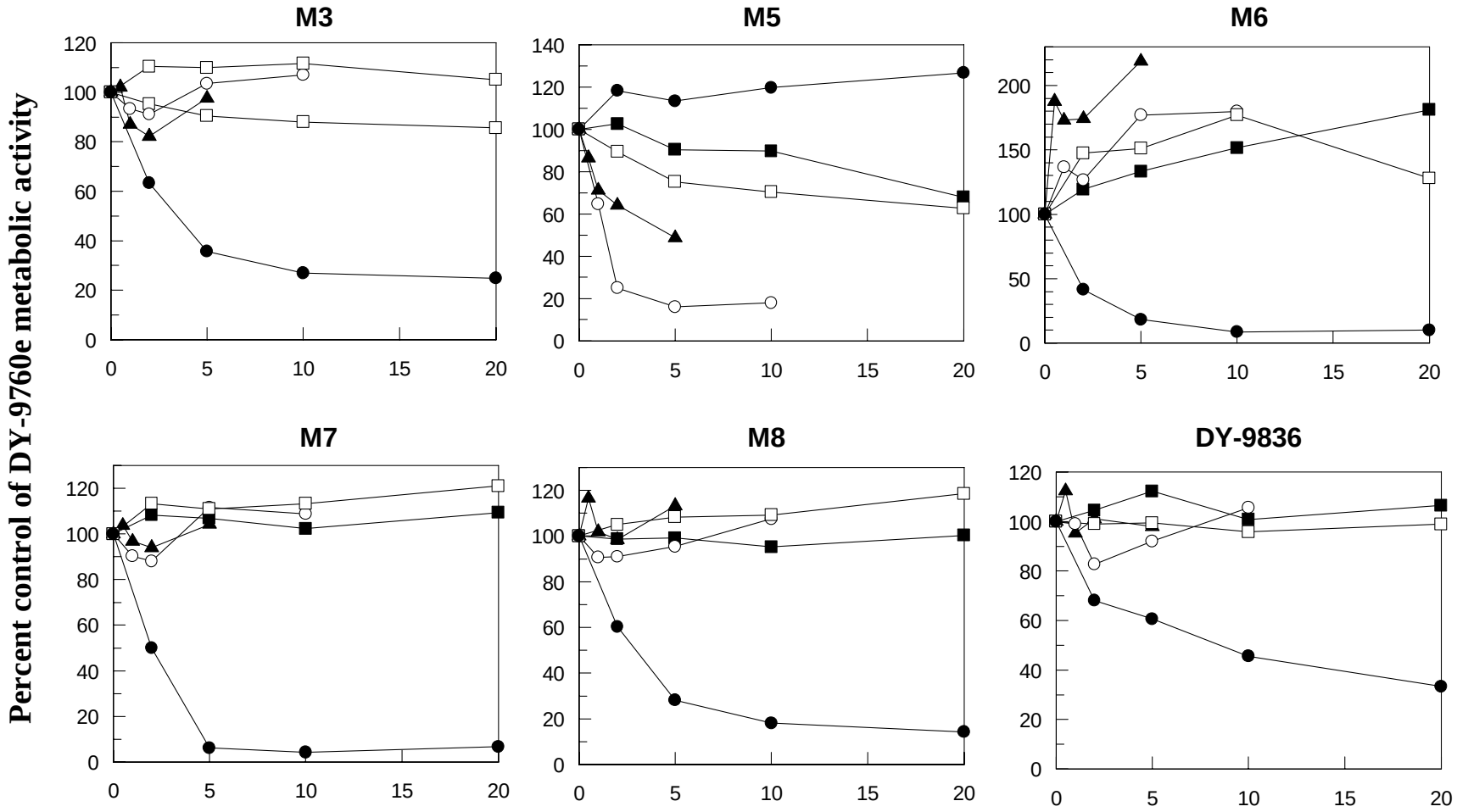

FIG.4

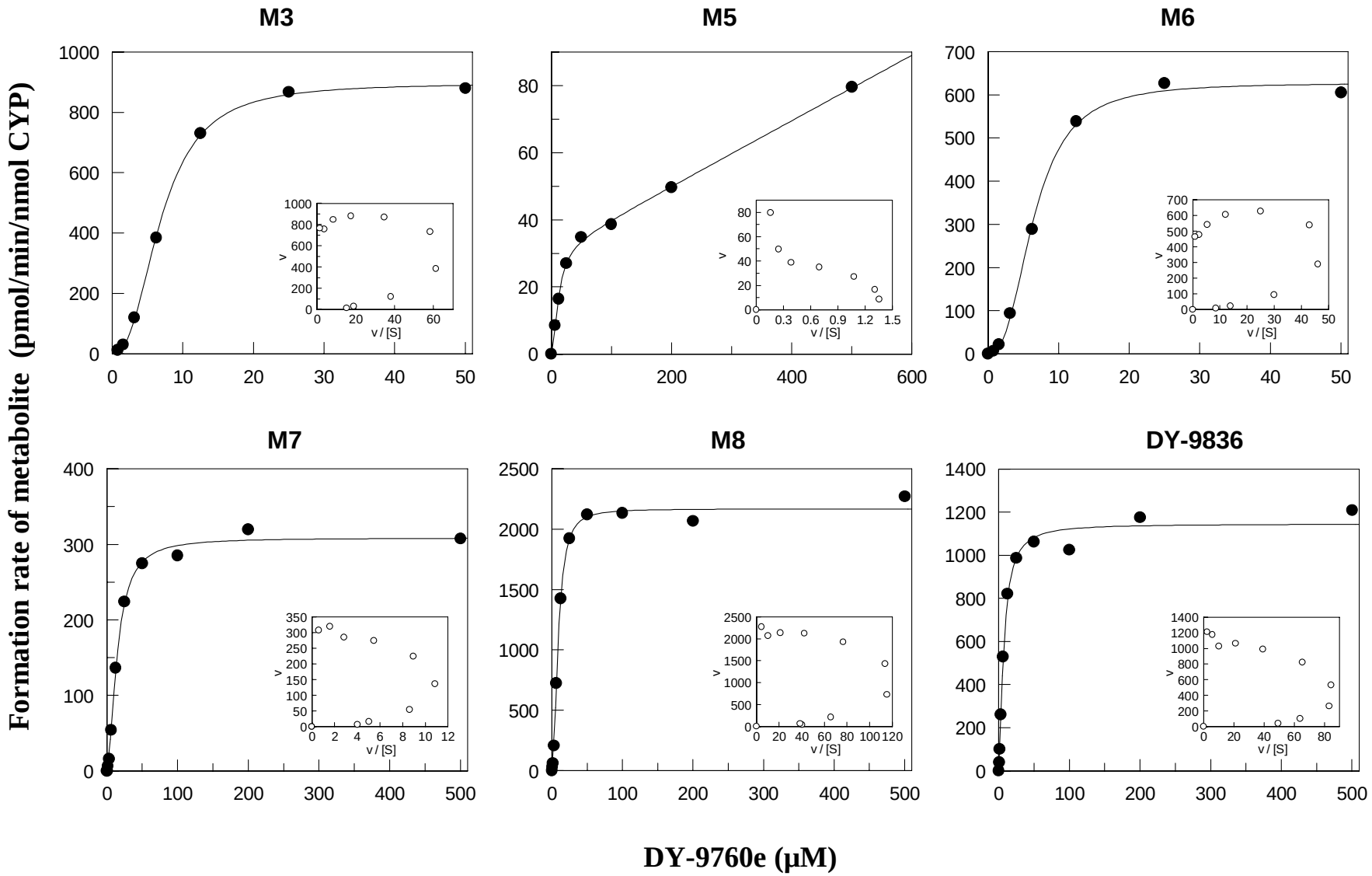

FIG.5